Supporting Information

Welding Partially Reduced Graphene Oxides by MOFs into Micro-Mesoporous Hybrids for High-Performance Oil Absorption

Lu Sun[a], *Jun Tang**[,a]

a. Dr. L. Sun, Prof. J. Tang,
Department of Polymer Science, Jilin University, Changchun 130012, China
E-mail: Jun Tang: chemjtang@jlu.edu.cn

A. Experimental Details

Materials. 2-amino-1,4-benzenedicarboxylic acid (ABDCA) (99 %), Zirconium (IV) chloride ($ZrCl_4$, 99.5 %), hydriodic acid (HI, 55 wt%), Rhodamine B (97 %), Nile red, and graphite flake powder (100 mesh) were obtained from Sigma Aldrich Chemical Co (Shanghai, China). Tetrahydrofuran, hexane, petroleum ether, ether, methylene chloride, toluene,chloroform, and N, N-dimethylformamine (DMF) were obtained from Beijing Chemical Industry Group C. Ltd. Beijing, China. All the chemicals were used as supplied without further purification. Melamine foams (MFs) were purchased from Xuxian Trading (Shanghai, China). Water with a resistivity of 18 $M\Omega \cdot cm^{-1}$ was prepared using a Millipore Milli-Q system and used in all experiments.

Synthetic procedure for UiO-66-NH_2 nanoparticles. UiO-66-NH_2 nanoparticles were prepared according to the refered literature[1]. $ZrCl_4$ (0.6 g) and ABDCA (0.466 g) were dissolved in DMF (120 mL), followed by 24 h incubation at 120 ^oC under stirring. After the reaction solutions were cooled down, the resulting UiO-66-NH_2 nanoparticles were collected by means of centrifugation and redispersed

in DMF. After repeating the centrifugation/redispersion cycle for several times, the UiO-66-NH_2 nanoparticles were dried at 60 ^oC in vacuo overnight.

Synthesis of Partially Reduced Graphite Oxide (GOs). GOs were synthesized by oxidation of graphite flakes according to a modified Hummers method[2]. PRGOs were produced according to the protocol reported in lieteruare[3]. Typically, as-prepared GOs (20 mg) were dispersed in aqueous solution of HI (55 wt%), followed by incubation at 90 °C for 1 min, followed to wash by ethanol for 3 times and water for 3 times. Afterwards, the resulting powers were stored in a oven at 200 ^oC for 30 min, which ensured the conversion of the GOs to PRGOs. The resulting PRGOs were dried at 60 ^oC in vacuo for further use.

Synthesis of GO@UiO-66-NH_2 and PRGO@UiO-66-NH_2 hybrids. 20 mg of as-prepared GOs or PRGOs were dispersed in 10 mL of chloroform with the aid of sonication. 60 mg of $ZrCl_4$ and 46.6 mg of ABDCA were dissolved in 120 mL of DMF. The resulting $ZrCl_4$/ABDCA solution in DMF and the GO or PRGO dispersion in chloroform were mixed under stirring, followed by incubation at 120 ^oC for 24 h under stirring. After being cooled down to room temperature, the resulting reaction solution was submitted to centrifugation at speed of 8000 rpm to collect the hybrids. The collected hybrids were purified by repeating the centrifugation/dispersion cycle in DMF for 3 times. The resulting hybrids were dried at 60 ^oC in vacuo for further use.

Synthesis of composite MFs. As-prepared UiO-66-NH_2 nanoparticles, GOs, GO@UiO-66-NH_2 hybrids, and PRGO@UiO-66-NH_2 hybrids, respectively, were dispersed in water to produce the relatively stable dispersion with the solid content of

3 mg mL^{-1}. Subsequently, the blocks of pristine MFs with dimensions (2×2×2) cm^3 were immersed into the resulting aqueous dispersions and thoroughly impregnated with the aqueous dispersions. Then the MF blocks were taken out and placed in plastic centrifugal tubes (50 mL), followed by centrifugation at 3,000 rpm for 2 min to remove the aqueous dispersions from the macroporous structures of the MF blocks. The resulting composite MF blockes were dried at 60 °C for 1 h, yielding composite MF blocks with UiO-66-NH_2 nanoparticles, GOs, GO@UiO-66-NH_2 hybrids, and PRGO@UiO-66-NH_2 hybrids coated on their macroporous surfaces.

In order to produce PRGO – laden MFs, as-prepared GO – laden MF blocks were placed in the aqueous solutions of HI (55 wt%). After 1 min incubation at 90 ^oC, the composite MF blocks were taken out from the HI solution, followed to wash by ethanol for 3 times and water for 3 times. Afterwards, the composite MF blocks were stored in a oven at 200 ^oC for 30 min, which ensured complete conversion of the GOs loaded therein to PRGOs.

Characterization. Scanning electron microscopy (SEM) imaging and energy dispersive spectroscopic (EDS) elementary mapping were performed on a Hitachi FE-SEM S-4800 scanning electron microscope with an acceleration voltage of 3kV. Transmission electron microscopy (TEM) was carried out on a JEM-2100F field emission electron microscope with an acceleration voltage of 200 kV. Powder X-ray diffraction (XRD) patterns were collected on a PANalytical B.V. Empyrean powder diffraction, in which data were collected from 5 to 45 º at a scan rate of 15 º/min. X-ray photoelectron spectroscopy (XPS) was performed on a PHI 5000 Versa Probe II

scanning XPS microprobe from Physical Electronics, using X-ray radiation from an Al source equipped with a monochromator. Nitrogen sorption isotherms were measured by using a Quantachrome Autosorb-1C surface area and pore size analyzer at 77 K. Prior to nitrogen sorption isotherm measurement, the samples were dried in vacuum (~1 $\times 10^{-5}$ Torr) at room temperature for 1 h, at 80 °C for 6 h and 100 °C for 12 h. Water contact angles were measured on a Contact Angle Measuring Instrument (KRUSS, DSA30). Fluorescent photographs were taked under a UV lamp (WFH-204B, Shanghai Precision Instrument Co., Ltd).

B. SupplementaryMaterials

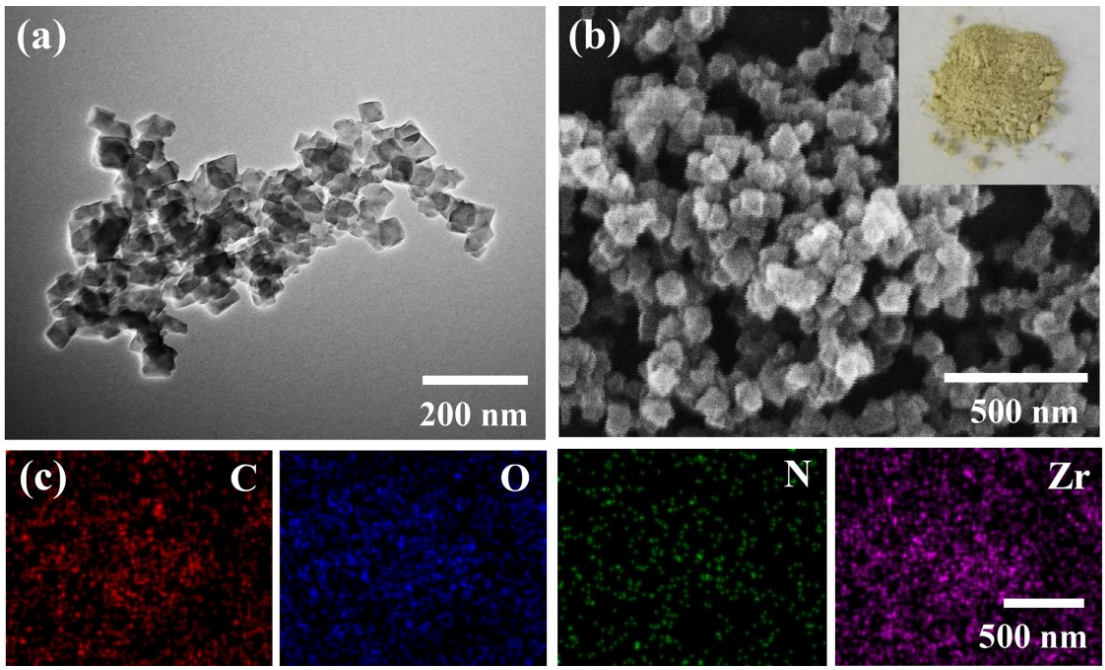

Figure S1. TEM (a), SEM (b) and EDS elemental mapping images (c) of as-prepared UiO-66-NH_2 nanoparticles. The inset in Figure b shows a photo of the UiO-66-NH_2 nanoparticle powders.

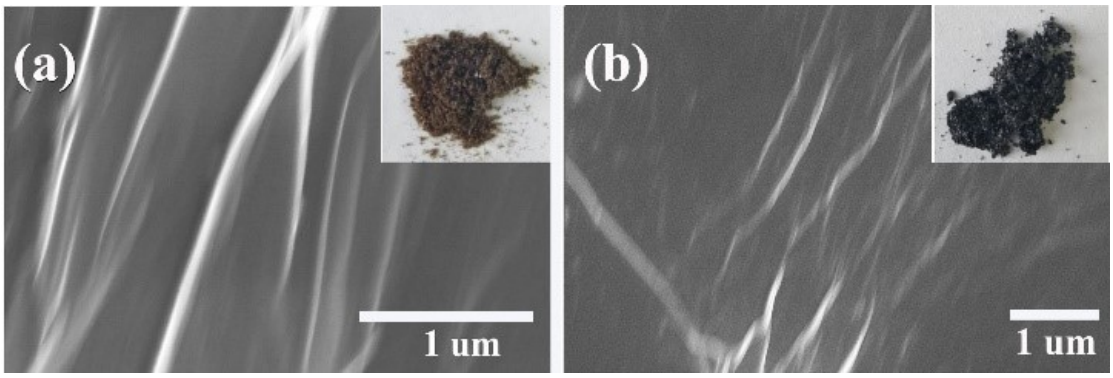

Figure S2. SEM (a, b) of as-prepared GOs and PRGOs. The insets in Figure a and b show the photos of the GO and PRGO powders.

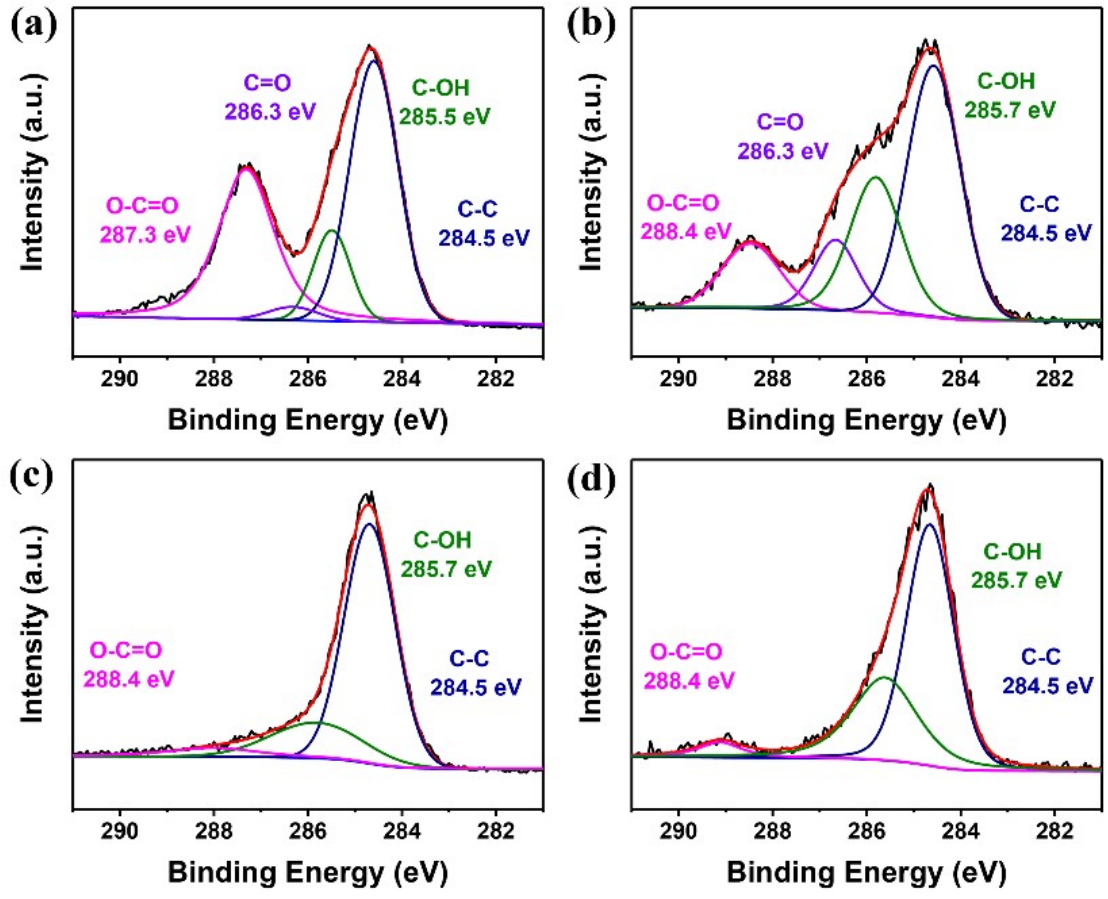

Figure S3. High-resultion XPS spectra of as-prepared GOs (a), GO@UiO-66-NH_2 hybrids (b), PRGOs (c) and PRGO@UiO-66-NH_2 hybrids (d), in which the C 1s signals are deconvoluted into the peaks of O-C=O (peak curves), C=O (purple curves), C-OH (green curves), and C-C (blue curves) moieties.

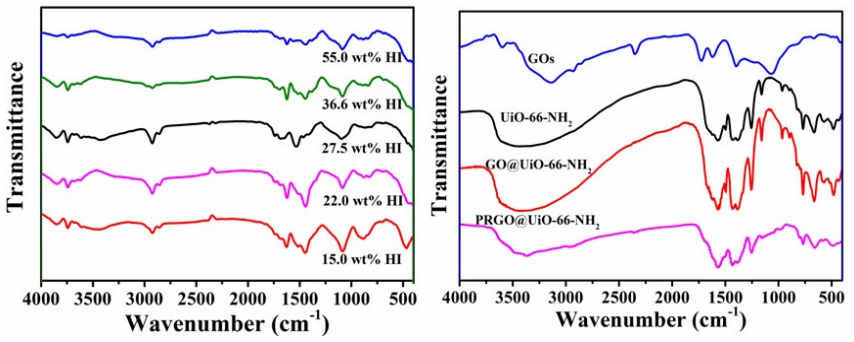

Figure S4. (a) The FT-IR spectrum of the powders of PRGOs treated with different concentrations of HI from 15.7 wt% - 55 wt% and (b) powders of GOs (blue curve), UiO-66-NH_2 (black curve), GO@UiO-66-NH_2 (red curve) and PRGO@UiO-66-NH_2 (pink curve).

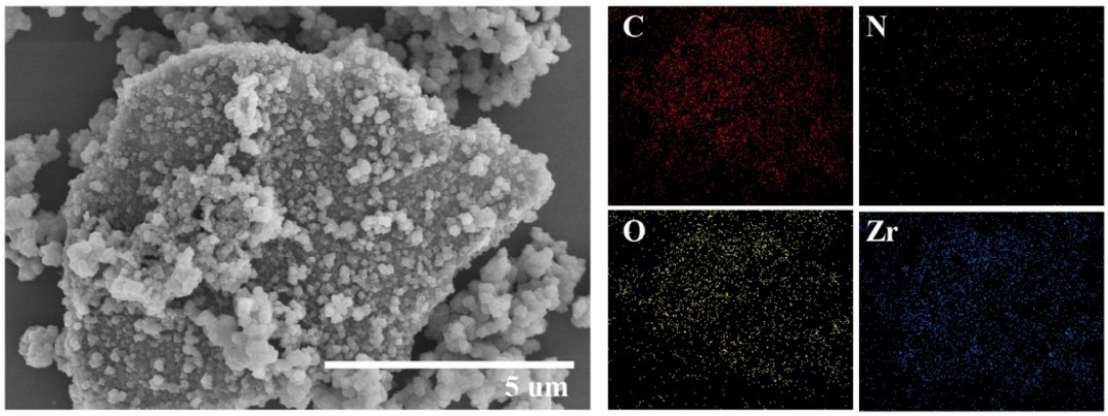

Figure S5. SEM and EDS elemental mapping impages of as-prepared GO@UiO-66-NH_2 hybrids.

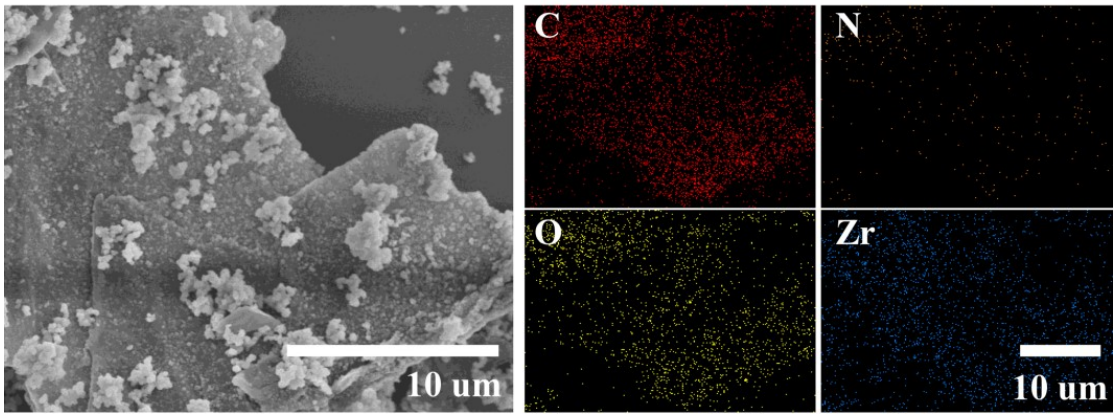

Figure S6. SEM and EDS elemental mapping images of PRGO@UiO-66-NH_2 hybrids.

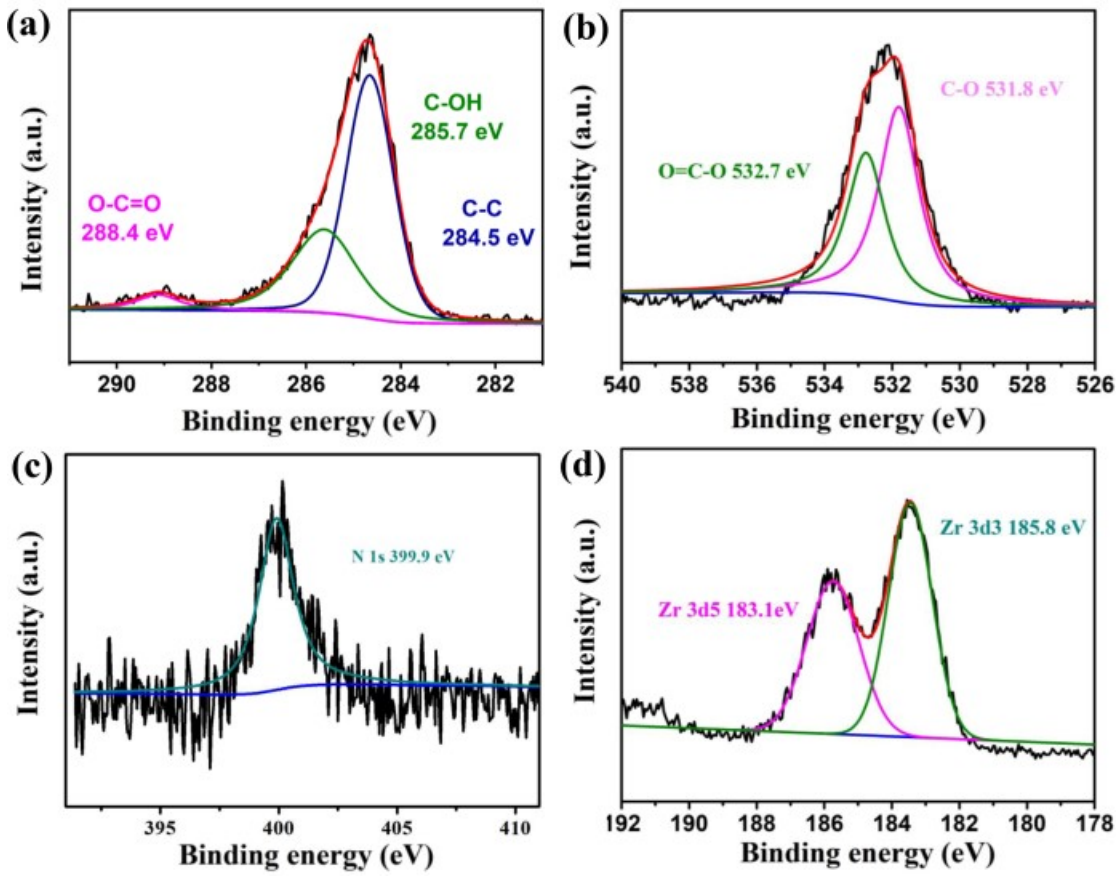

Figure S7. XPS spectra of (a) C1s, (b) O1s, (c) N 1s, and (d) Zr 3d signals of PRGO@UiO-66-NH_2 hybrids.

Table S1. Element Content Distribution (XPS).

PP At.%	GOs	PRGOs	GO@UiO-66-NH_2	PRGO@UiO-66-NH_2
C 1s	72.31	89.31	51.56	63.95
O 1s	27.69	10.69	31.49	24.48
N 1s	0	0	11.96	5.2
Zr 3d	0	0	4.98	6.37

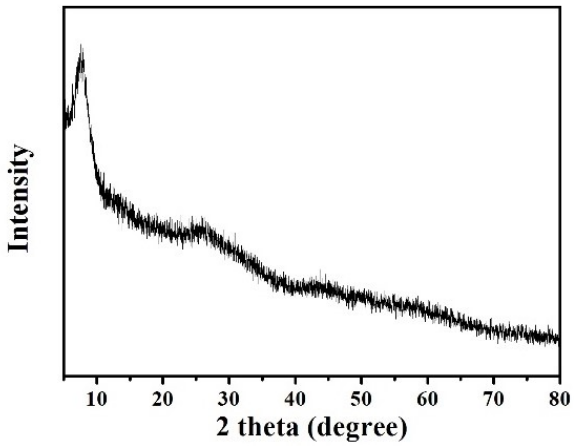

Figure S8. XRD pattern of PRGO@UiO-66-NH_2 hybrids derived from as-prepared GO@UiO-66-NH_2 hybrids via HI reduction, in which the peaks at 12.2°, 25.8°, and 43.5°, characteristic of UiO-66-NH_2 nanocrystals, disappeared, indicative of poor crystallinity of the resulting UiO-66-NH_2 framework.

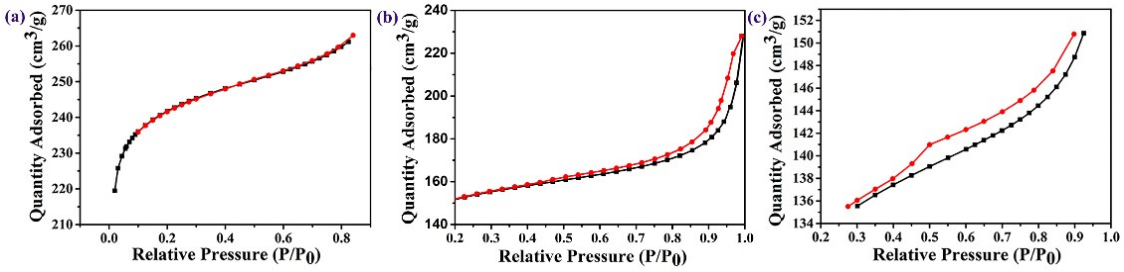

Figure S9. Nitrogen adsorption (black curves)-desorption (red curves) isotherms of as-prepared UiO-66-NH_2 nanoparticles (a), GO@UiO-66-NH_2 hybrids (b) and (c) PRGO@UiO-66-NH_2 hybrids (c), which highlights the difference in the adsorption (black curves)/desorption (red curves) hysteresis.

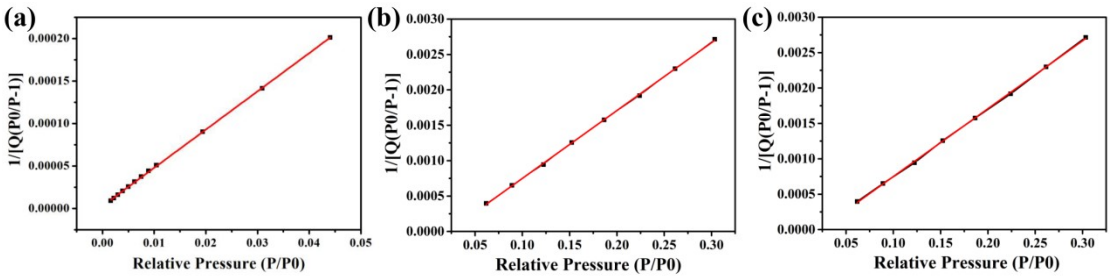

Figure S10. BET surface area plots of as-prepared UiO-66-NH_2 nanoparticles (a), GO@UiO-66-NH_2 hybrids (b) and PRGO@UiO-66-NH_2 hybrids (c).

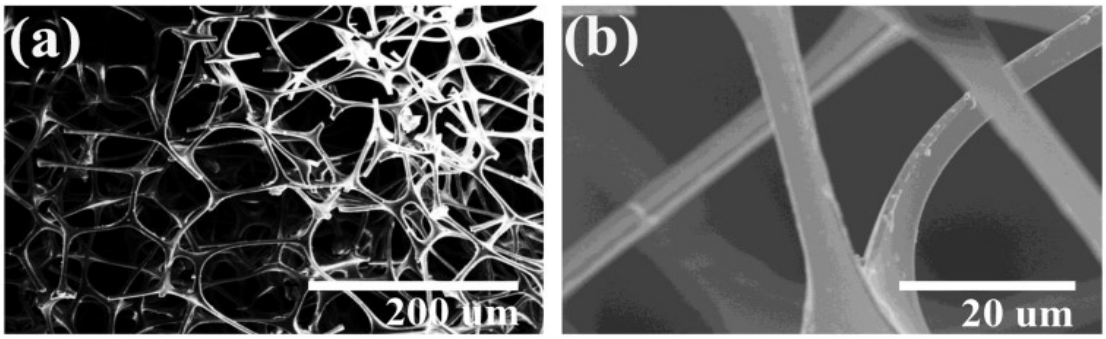

Figure S11. Low (a) and High magnification (b) SEM images of MFs.

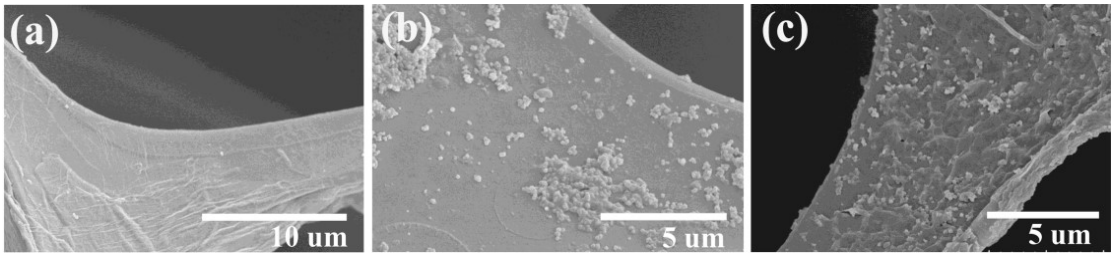

Figure S12. High magnification SEM images of MFs loaded with as-prepared GO (a), UiO-66-NH_2 nanoparticles (b) and GO@UiO-66-NH_2 hybrids (c) on their macropores.

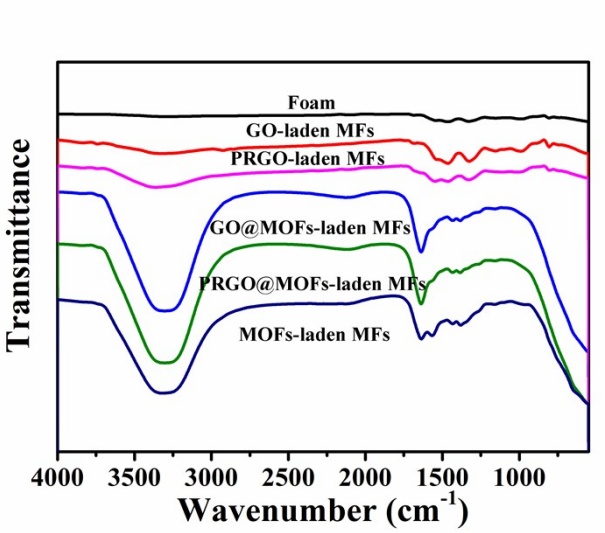

Figure S13. The FT-IR spectrum of a block of pristine MFs (black curve), and the blocks of the composite MF loaded by GOs (red curve), PRGOs (pink curve), GO@UiO-66-NH_2 hybrids (light blue curve), PRGO@UiO-66-NH_2 hybrids (green curve), and UiO-66-NH_2 nanoparticles (dark blue curve).

Figure S14. Photo of a water droplet (2 μL) completely infused into the macroporous structures of a pristine MF block after being placed atop in air; its appearant $\theta_{w/a}$ of 0°.

Figure S15. Photo of an oil droplet (2 μL) completely infused into the macroporous structures of a block of PRGO@UiO-66-NH_2 – laden MF after being placed atop in air; its appearant $\theta_{o/a}$ of 0°.

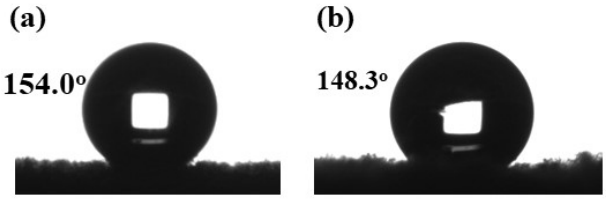

Figure S16. The water droplets of 2 μL on MFs loaded with PRGO@UiO-66-NH_2 hybrids before oil adsorption (a) and after ten cycles of oil adsorption and water repellence (b). The photos are taken after 120s after the water droplets are placed on the MF surfaces. The corresponding $\theta_{w/a}$ values are marked in the photos.

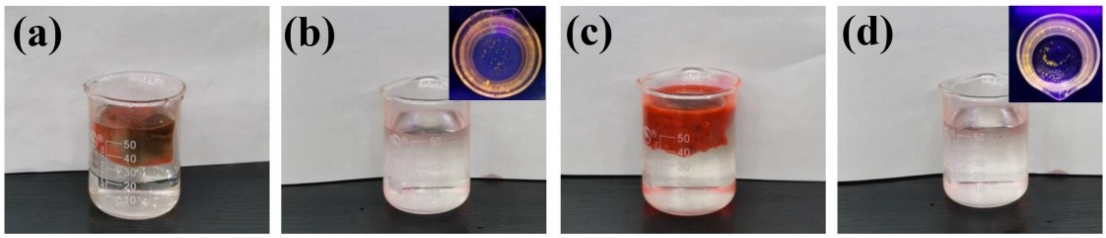

Figure S17. A series of photos taken after a composite MF block loaded with GO@UiO-66-NH_2 hybrids is placed on an oil/water biphasic mixture (a) and it is able to absorb the large fraction of the oil layer spilt on the water surface within 5 s (b), and then after the absorbed oil is squeezed out, the same composite MF block is

placed on a new oil/water biphasic mixture (c) and is still able to absorb the large fraction of the oil layer from the water surface within 5s (d). The oil phase is vegetable oil and stained by Nile red. After oil absorption by the composite MF block, the fluorescence of Nile red is clearly visible, indicative of incomplete oil absorption by GO@UiO-66-NH_2 – laded MFs from water (b and d).

Table S2. The hydrophobicity and stability of MFs with the changes of concentration of HI as reducing agent.

Concentration of HI (wt %)	15.7	22.0	27.5	36.6	55.0
PRGO-laden MFs ($\theta_{w/a}$)	117.1°	123.5°	125.6°	128.5°	131.6°
After 2 min ($\theta_{w/a}$)	103.3°	116.7°	118.3°	125.6°	130.7°
PRGO@MOFs-laden MFs ($_{w/a}$)	133.6°	138.2°	144.4°	150.2°	154.2°
After 2 min ($\theta_{w/a}$)	122.9°	128.5°	138.5°	148.0°	154.0°

References

[1] B. Ghalei, K. Sakurai, Y. Kinoshita, K. Wakimoto, Ali P. Isfahani, Q. Song, K. Doitomi, S. Furukawa, H. Hirao, H. Kusuda, S. Kitagawa and E. Sivaniah, *Nature Energy* 2017, ***2***, 17086.

[2] a) J. Ge, H. B, Yao, H. W, X. F, Yu, Y. X, Yan, L. B, Mao, H. H, Li, S. S, Li and S. H, Yu, *Nano Energy* **2013**, *2*, 505-513; b) D. Li, M. B. Muller, S. Gilje, R. B. Kaner and G. G. Wallace, *Nat Nanotechnol,* 2008, ***3***, 101-105.

[3] J. Ge, L. A. Shi, Y. C. Wang, H. Y. Zhao, H. B. Yao, Y. B. Zhu, Y. Zhang, H. W. Zhu, H. A. Wu and S. H. Yu, *Nat Nanotechnol,* 2017, ***12***, 434-440.